

The surface detector array of the Telescope Array experiment

T. Abu-Zayyad^a, R. Aida^b, M. Allen^a, R. Anderson^a, R. Azuma^c,
 E. Barcikowski^a, J. W. Belz^a, D. R. Bergman^a, S. A. Blake^a, R. Cady^a,
 B. G. Cheon^d, J. Chiba^e, M. Chikawa^f, E. J. Cho^d, W. R. Cho^g, H. Fujii^h,
 T. Fujiiⁱ, T. Fukuda^c, M. Fukushima^{j,t}, D. Gorbunov^k, W. Hanlon^a,
 K. Hayashi^c, Y. Hayashiⁱ, N. Hayashida^l, K. Hibino^l, K. Hiyama^j,
 K. Honda^b, T. Iguchi^c, D. Ikeda^j, K. Ikuta^b, N. Inoue^m, T. Ishii^b,
 R. Ishimori^c, D. Ivanov^{a,n}, S. Iwamoto^b, C. C. H. Jui^a, K. Kadota^o,
 F. Kakimoto^c, O. Kalashev^k, T. Kanbe^b, K. Kasahara^p, H. Kawai^q,
 S. Kawakamiⁱ, S. Kawana^m, E. Kido^j, H. B. Kim^d, H. K. Kim^g, J. H. Kim^d,
 J. H. Kim^r, K. Kitamoto^f, K. Kobayashi^e, Y. Kobayashi^c, Y. Kondo^j,
 K. Kuramotoⁱ, V. Kuzmin^k, Y. J. Kwon^g, S. I. Lim^s, S. Machida^c,
 K. Martens^t, J. Martineau^a, T. Matsuda^h, T. Matsuura^c, T. Matsuyamaⁱ,
 J. N. Matthews^a, I. Myers^a, M. Minaminoⁱ, K. Miyata^e, H. Miyauchiⁱ,
 Y. Murano^c, T. Nakamura^u, S. W. Nam^s, T. Nonaka^{j,*}, S. Ogioⁱ,
 M. Ohnishi^j, H. Ohoka^j, K. Oki^j, D. Oku^b, T. Okudaⁱ, A. Oshimaⁱ,
 S. Ozawa^p, I. H. Park^s, M. S. Pshirkov^v, D. Rodriguez^a, S. Y. Roh^r,
 G. Rubtsov^k, D. Ryu^r, H. Sagawa^j, N. Sakuraiⁱ, A. L. Sampson^a,
 L. M. Scottⁿ, P. D. Shah^a, F. Shibata^b, T. Shibata^j, H. Shimodaira^j,
 B. K. Shin^d, J. I. Shin^g, T. Shirahama^m, J. D. Smith^a, P. Sokolsky^a,
 T. J. Sonley^a, R. W. Springer^a, B. T. Stokes^a, S. R. Stratton^{a,n},
 T. A. Stroman^a, S. Suzuki^h, Y. Takahashi^j, M. Takeda^j, A. Taketa^w,
 M. Takita^j, Y. Tameda^j, H. Tanakaⁱ, K. Tanaka^x, M. Tanaka^h,
 S. B. Thomas^a, G. B. Thomson^a, P. Tinyakov^{k,v}, I. Tkachev^k, H. Tokuno^c,
 T. Tomida^b, S. Troitsky^k, Y. Tsunesada^c, K. Tsutsumi^c, Y. Tsuyuguchi^b,
 Y. Uchihori^y, S. Udo^l, H. Ukai^b, G. Vasiloff^a, Y. Wada^m, T. Wong^a,
 M. Wood^a, Y. Yamakawa^j, H. Yamaoka^h, K. Yamazakiⁱ, J. Yang^s,
 S. Yoshida^q, H. Yoshii^z, R. Zollinger^a, Z. Zundel^a

^aUniversity of Utah, High Energy Astrophysics Institute, Salt Lake City, Utah, USA

^bUniversity of Yamanashi, Interdisciplinary Graduate School of Medicine and
Engineering, Kofu, Yamanashi, Japan

*Corresponding author

Email address: nonaka@icrr.u-tokyo.ac.jp (T. Nonaka)

33 ^c*Tokyo Institute of Technology, Meguro, Tokyo, Japan*
34 ^d*Hanyang University, Seongdong-gu, Seoul, Korea*
35 ^e*Tokyo University of Science, Noda, Chiba, Japan*
36 ^f*Kinki University, Higashi Osaka, Osaka, Japan*
37 ^g*Yonsei University, Seodaemun-gu, Seoul, Korea*
38 ^h*Institute of Particle and Nuclear Studies, KEK, Tsukuba, Ibaraki, Japan*
39 ⁱ*Osaka City University, Osaka, Osaka, Japan*
40 ^j*Institute for Cosmic Ray Research, University of Tokyo, Kashiwa, Chiba, Japan*
41 ^k*Institute for Nuclear Research of the Russian Academy of Sciences, Moscow, Russia*
42 ^l*Kanagawa University, Yokohama, Kanagawa, Japan*
43 ^m*Saitama University, Saitama, Saitama, Japan*
44 ⁿ*Rutgers University, Piscataway, USA*
45 ^o*Tokyo City University, Setagaya-ku, Tokyo, Japan*
46 ^p*Waseda University, Advanced Research Institute for Science and Engineering,*
47 *Shinjuku-ku, Tokyo, Japan*
48 ^q*Chiba University, Chiba, Chiba, Japan*
49 ^r*Chungnam National University, Yuseong-gu, Daejeon, Korea*
50 ^s*Ewha Womans University, Seodaemun-gu, Seoul, Korea*
51 ^t*University of Tokyo, Institute for the Physics and Mathematics of the Universe,*
52 *Kashiwa, Chiba, Japan*
53 ^u*Kochi University, Kochi, Kochi, Japan*
54 ^v*University Libre de Bruxelles, Brussels, Belgium*
55 ^w*Earthquake Research Institute, University of Tokyo, Bunkyo-ku, Tokyo, Japan*
56 ^x*Hiroshima City University, Hiroshima, Hiroshima, Japan*
57 ^y*National Institute of Radiological Science, Chiba, Chiba, Japan*
58 ^z*Ehime University, Matsuyama, Ehime, Japan*

59 **Abstract**

The Telescope Array (TA) experiment, located in the western desert of Utah, USA, is designed for observation of extensive air showers from extremely high energy cosmic rays. The experiment has a surface detector array surrounded by three fluorescence detectors to enable simultaneous detection of shower particles at ground level and fluorescence photons along the shower track. The TA surface detectors and fluorescence detectors started full hybrid observation in March, 2008. In this article we describe the design and technical

features of the TA surface detector.

60 *Keywords:* Ultra-high energy cosmic rays; Telescope Array experiment;
61 Extensive air shower array

62 **1. Introduction**

63 The main aim of the Telescope Array (TA) experiment [1] is to explore
64 the origin of ultra high energy cosmic rays (UHECR) using their energy
65 spectrum, composition and anisotropy. There are two major methods of ob-
66 servation for detecting cosmic rays in the energy region above $10^{17.5}$ eV. One
67 method which was used at the High Resolution Fly's Eye (HiRes) experiment
68 is to detect air fluorescence light along air shower track using fluorescence
69 detectors. The other method, adopted by the AGASA experiment, is to de-
70 tect air shower particles at ground level using surface detectors deployed over
71 a wide area (~ 100 km²).

72 The AGASA experiment reported that there were 11 events above 10^{20}
73 eV in the energy spectrum [2, 3]. However, the existence of the GZK cutoff
74 [4, 5] was reported by the HiRes experiment [6]. The Pierre Auger experiment
75 confirmed the suppression on the cosmic ray flux at energy above 4×10^{19} eV
76 [7] using an energy scale obtained by fluorescence light telescopes (FD). The
77 contradiction between results from fluorescence detectors and those from sur-
78 face detector arrays (SD) remains to be investigated by having independent
79 energy scales using both techniques. Hybrid observations with SD and FD
80 enable us to compare both energy scales. Information about core location
81 and impact timing from SD observation improves accuracy of reconstruction
82 of FD observations. Observations with surface detectors have a nearly 100%

83 duty cycle, which is an advantage especially for studies of anisotropy. Cor-
84 relations between arrival directions of cosmic rays and astronomical objects
85 in this energy region should give a key to exploring the origin of UHECR [8]
86 and their propagation in the galactic magnetic field.

87 In this article we describe the design and technical features of the TA
88 surface detector.

89 **2. Telescope Array experiment**

90 The TA site is located in the desert about 1400 m above sea level cen-
91 tered at 39.3°N and 112.9°W in Millard County, Utah, USA, about 200 km
92 southwest of Salt Lake City. A control center to support construction and
93 operation of the TA instruments is in the city of Delta located near the north-
94 east side of the array. The experiment is aimed at observing cascade showers
95 induced by cosmic rays above 10^{19} eV. The altitude of the experimental site
96 is optimal for observing particle showers at nearly maximum development of
97 the cascade. For hybrid observation the site also needed to be located in a
98 semi-desert area with less light pollution from the town. The dry climate
99 allows us to have a high duty cycle for FD-SD hybrid exposure; about 10%
100 of real time.

101 Below we describe the major advantages of the TA experiment:

102 1) The TA experiment utilizes plastic scintillators similar to AGASA ex-
103 periment. For energies of about 10^{20} eV, more than 90% of the primary
104 energy is absorbed as the electromagnetic component (e^+, e^- and γ) in the
105 air. Plastic scintillators are sensitive to all charged particles, and the en-
106 ergy measurement is less affected by the difference of the details of unknown

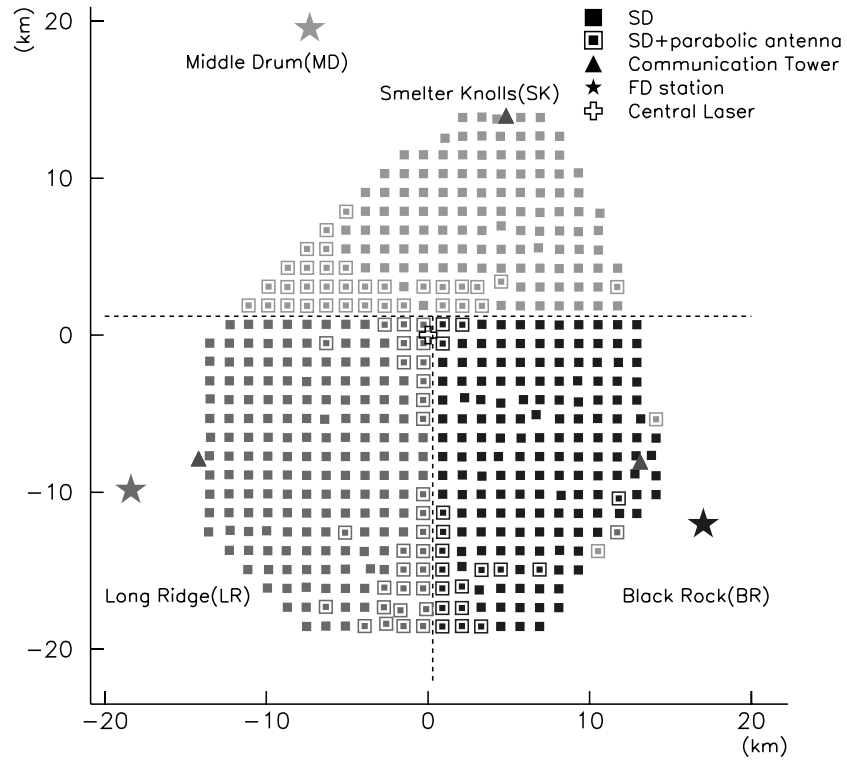


Figure 1: Layout of the Telescope Array in Utah, USA. Squares denote 507 SDs. There are three subarrays controlled by three communication towers denoted by triangles. The three star symbols denote the FD stations.

107 hadron interactions and the primary composition. 2) The HiRes-I telescope
108 system was partially moved to the Middle Drum (MD) hill in TA site and
109 installed as one of the three FD stations after the HiRes experiment was shut
110 down in 2006 [9]. Using an energy spectrum obtained with MD station data,
111 it is possible to cross-check the new TA FD data and analysis method. The
112 surface detector observes lateral distribution of the shower particle. Energy
113 deposition at a certain distance from shower core is used as an estimator of
114 the energy by comparing with air shower Monte Carlo simulation. It is pos-
115 sible to compare the estimated energy with that obtained from longitudinal
116 shower development observed by FD data analysis.

117 3) In addition to the conventional calibration and monitor system, we plan to
118 perform absolute end-to-end calibration of a fluorescence telescope by using
119 pseudo air shower events that are induced by electron beams with known to-
120 tal energy from a compact electron linear accelerator at the TA site [10, 11].
121 As described above, the TA experiment is well-balanced to determine the
122 energy of air shower events.

123 4) The anisotropy of arrival directions of ultra-high energy cosmic rays is
124 being studied in the northern hemisphere where the effect of the galactic
125 magnetic field is smaller than that in the southern hemisphere. A typical
126 angular resolution of TA SD array is better than 1.5° for the shower above
127 10 EeV [12].

128 **3. Surface detector array**

129 The SD array consists of 507 detector units, which were deployed in a
130 square grid with 1.2 km spacing to cover a total area of approximately 700

131 km². Fig. 1 shows a layout of the TA experiment. Each surface detector
132 has a plastic scintillation counter of 3 m² in size, and transmits SD data
133 via a wireless LAN modem. As shown in Fig. 1, the SD array is divided
134 into three subarrays each controlled by its trigger-decision electronics at the
135 communication tower. The Long Ridge (LR), Black Rock (BR), and Smelter
136 Knolls (SK) subarrays have 189, 170 and 148 SDs respectively. (The numbers
137 of SDs in LR, BR and SK from March 2008 to November 2009 were 207, 190
138 and 110 respectively.) All detectors are powered by solar panels and batteries
139 [13]. For events with energies beyond 10¹⁹ eV and with zenith angles below
140 45 degrees, the trigger efficiency reaches ~100% and the aperture is 1100
141 km²·sr. The observed energy region for the TA experiment has sufficient
142 overlap with those for the previous experiments of UHECR.

143 *3.1. Surface detector*

144 The TA detector will operate for more than 10 years and must be de-
145 signed to survive the expected conditions at the site. The detector must be
146 robust and durable for long-term exposure to the desert environment where
147 the detector temperature ranges from -20°C to +50°C with large diurnal
148 variations. And the system requires detailed monitoring and periodic cali-
149 brations to track variations of detector response along time.

150 Fig. 2 shows one of the deployed SDs that communicate with the commu-
151 nication tower placed at Smelter Knolls (SK), a nearby hill. A communication
152 antenna (ADAF2414; ADTEC Co.) with adjustable height is mounted on
153 a 3-m long iron pole. A square solar panel 1 m on one side is mounted on
154 the platform to supply power to the electronics. Front-end electronics and a
155 battery are contained in a box made with 1.2 mm thick stainless steel. The

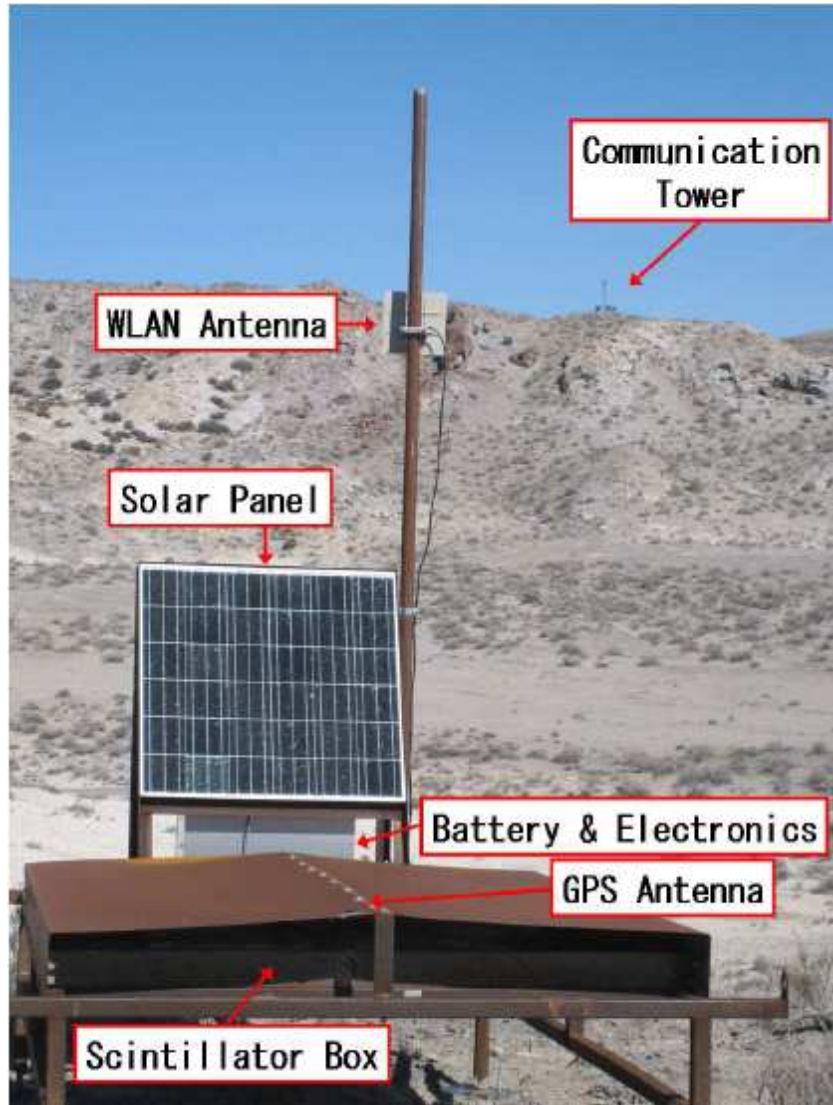


Figure 2: A deployed SD in the field. The electronics box and scintillator box are on the iron frame. An electronics unit is installed under the solar panel, and the scintillator box is mounted on the platform under the roof.

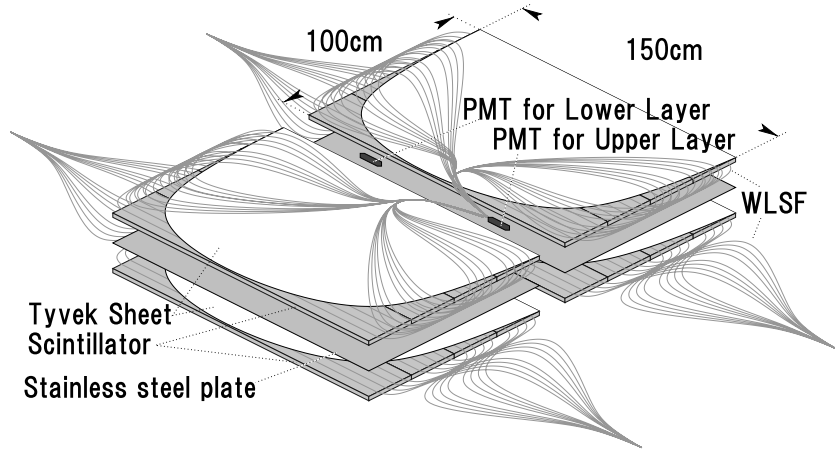


Figure 3: Inside of a scintillator box with scintillator plates, WLS fibers and PMTs. A total of 104 WLS fibers are laid on each layer to collect and transmit scintillation light to a PMT [14].

156 box is mounted under the solar panel. The box that contains the scintillators
 157 and photomultiplier tubes (PMTs) is mounted under the 1.2-mm thick iron
 158 roof to protect the detector from large temperature variations.

159 Fig. 3 shows a schematic of the inside of a scintillator box. Each surface
 160 detector consists of two layers of plastic scintillator. Each layer of scintillator
 161 has an area of 3 m^2 and a thickness of 1.2 cm. A Stainless-steel plate has
 162 1 mm in thickness and is inserted between the layers. As shown in Fig. 3,
 163 each scintillator layer consists of 2 segments, and each segment consists of 4
 164 slabs. The size of one segment is $1.5 \text{ m} \times 1.0 \text{ m}$. The size of each slab is
 165 $1.5 \text{ m} \times 0.25 \text{ m}$ and thickness is 1.2 cm. On top side of the scintillator slab,
 166 there are grooves in parallel along the length of the slab. The span of grooves
 167 is 2.0 cm and the depth is 1.5 mm. Scintillation light is collected through
 168 104 wavelength-shifting (WLS) fibers (Y-11; Kuraray Co. Ltd.) that are

169 laid along each groove. Total length of a WLS fiber is 5 m. The fibers are
170 put in the grooves on the surfaces of the scintillator slabs without oil and
171 grease, and are fixed at both edges of the slabs with tape (polyester tape
172 #850 silver; 3M). The segment is wrapped with two layer of Tyvek (1073B;
173 Dupont Co.) sheet. Both ends of the fibers from a layer are bundled together
174 and connected to a PMT (9124SA; Electron Tubes Ltd.).

175 Each PMT is calibrated to obtain the relation of high voltage and gain.
176 Linearity between input light amount and output charge is also obtained
177 in the calibration [15]. Two LEDs (NSPB320BS; Nichia Corp.) are also
178 installed on the side of each layer to calibrate linearity of output for input
179 light. Scintillator plates and PMTs are contained in a 1.5 mm thick box made
180 of stainless steel (top cover is 1.5 mm thick, with a 1.2 mm thick bottom)
181 (TAITO Co. Ltd.).

182 *3.2. Detector Electronics*

183 Fig. 4 shows the detector electronics for a scintillator counter installed in
184 a stainless-steel box under the solar panel. The output signals from PMTs
185 are digitized by a 12bit FADC (AD9235RU- 65; Analog Devices Co.) with
186 a 50 MHz sampling rate on the CPU board (SH4; Renesas Electronics Co.).
187 Signals greater than approximately 0.3 minimum ionizing particles (MIP) are
188 stored in a memory buffer on CPU board as Level-0 trigger data. The stored
189 waveform is 2.56 μ sec long (128 FADC bins). Signals greater than 3.0 MIP
190 are stored as a Level-1 trigger event, which are sent to the trigger-decision
191 electronics at the communication tower for the subarray via a wireless LAN
192 modem (ADLINK540F; ADTEC. Co) using a custom-made communication
193 protocol [16]. The local trigger rates are \sim 750 Hz for the Level-0 trigger

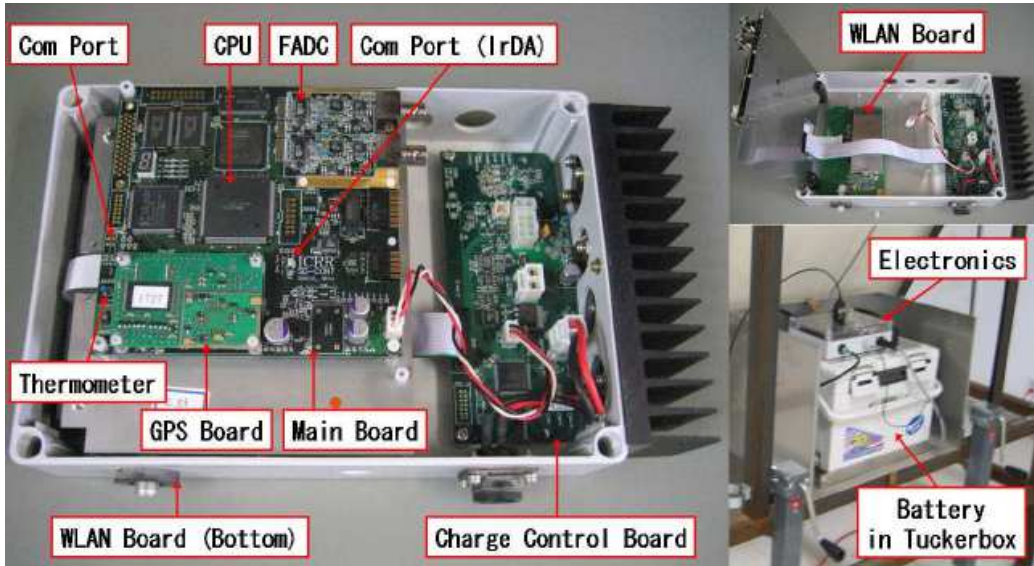


Figure 4: Detector electronics of the TA surface detector. The wireless LAN board is mounted under the main CPU board.

194 and ~ 30 Hz for the Level-1 trigger. In FPGA, the FADC pedestals are
 195 monitored every second to keep threshold values for the trigger. The pedestal
 196 value is defined as the average of FADC values within 160 nsec (8 FADC
 197 bins). The threshold value for Level-0 trigger is fixed to 15 counts above the
 198 average of pedestal. Triggered waveforms mostly from atmospheric particles
 199 are counted into histograms based on integrated count and maximum count
 200 of the waveform. For the monitoring of detector gain, the signal part of the
 201 waveform is integrated for 240 nsec (-80 nsec from trigger timing and up to
 202 +160 nsec after) and the values are accumulated into histograms for each
 203 layer of scintillator. The integrated FADC value and the maximum value
 204 of the signal waveform within $2.56 \mu\text{sec}$ are also accumulated in histograms.
 205 These are used for detector linearity monitoring. The synchronization of

206 electronics of the surface detectors is done by PPS signals received by GPS
207 units (Motorola M12+ oncore module). A time stamp with a precision of 20
208 nsec is created by the 50 MHz sub-clock on the main board. The total counts
209 of the sub-clock between PPS signals are also sent to the trigger-decision
210 electronics along with a Level-1 event list to correct the time stamp of the
211 waveform in later analysis. The power bases (PS1806/12F-02; Electrontube
212 Co. Ltd.) for PMTs are powered and controlled through DAC on the detector
213 electronics. Each SD unit described above is powered by one solar panel
214 (KC125TJ; KYOCERA Corp.) and one deep cycle battery (DCS100; C&D
215 technologies, Inc.). The solar panel has 125 W of charging power. The
216 battery has 100 Ah of capacity. The charging of the battery is controlled
217 by home made charge control board that works with main CPU board. The
218 solar panel system provides sufficient power required from the electronics (~ 5
219 W).

220 *3.3. Assembly and deployment*

221 Detector assembly is divided into two parts. First, two layers of plastic
222 scintillator are installed in the stainless-steel box and WLS fibers are laid
223 on each layer. To increase the light intensity, each layer of scintillator is
224 wrapped with two layers of Dupont Tyvek sheeting. Both ends of a bundle
225 of WLS fibers from a layer are glued together with epoxy inserted into an
226 acrylic sheath. The sheath is sized to fit the PMT surface. The ends of the
227 WLS fibers are smoothed with a grinder and polished after making a bundle
228 in the sheath. To ensure good optical contact, optical grease (Optseal; Shin-
229 Etsu Chemical Co. Ltd.) is also applied on the surface of the PMT. The
230 production rate of scintillator boxes was three boxes per day. In total 512

231 SD boxes were assembled in Japan and those boxes were shipped to Utah,
232 USA. Second, the final assembly of other components such as solar panels,
233 batteries, and electronics along with mounting these on to iron frames (T&D
234 Co. Ltd.) was performed at the control center in Delta. Each SD unit was
235 deployed to its location by using helicopter after transporting the units by
236 trucks with a flatbed trailer to staging areas accessible from existing roads
237 inside the TA site. From October 2006 to the end of February 2007, 485
238 surface detectors were deployed. A total of 503 SDs were deployed by the
239 end of December 2007. Additional 4 SDs were deployed in December 2008.

240 *3.4. Long-distance network for remote operation*

241 Fig. 5 shows one of the communication towers, which is located at Smelter
242 Knolls (SK) near the north edge of the SD array. The other two towers also
243 have the same size and are located on hills (Black Rock and Long Ridge)
244 near the western and eastern edges of the SD array, respectively. The com-
245 munication towers have the role of collecting trigger information from the
246 SDs and providing communications for the FD stations and CLF (Central
247 Laser Facility) [17] site for general purposes.

248 Fig. 6 shows the long-distance links for all the facilities and air fluores-
249 cence detectors in the entire TA site. The open triangles in Fig. 6 represent
250 the locations of the communication towers. The data collected from the SDs
251 are temporarily stored at the communication tower and regularly transferred
252 to Delta City through this network every 12 hours. There are two types of
253 antenna units (Canopy P2P100; Motorola Co. Ltd.) which are operated in
254 different frequency ranges. The tower-to-tower and tower-to-FD links are
255 operated at 5.7 GHz and the tower-to-SD links are operated at 2.4 GHz



Figure 5: The Smelter Knolls communication tower, one of three in the array. There are three stands each with four solar panels. Those stands contain batteries, data acquisition PC and network instruments for long distance link.

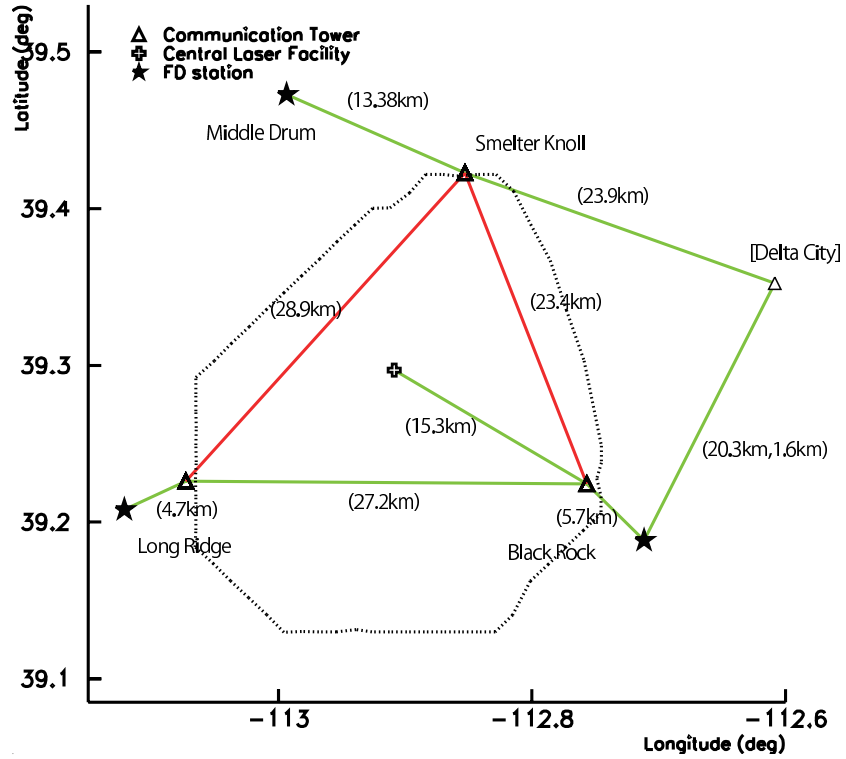


Figure 6: The long-distance links for all the facilities and three FD stations in the entire TA site. The open triangles represent the communication towers where the trigger-decision electronics for subarrays are installed. The lines that connect the towers and facilities represent the links between antennas. The red lines are used for trigger decision. The dotted line represents the border of the entire surface detector array.

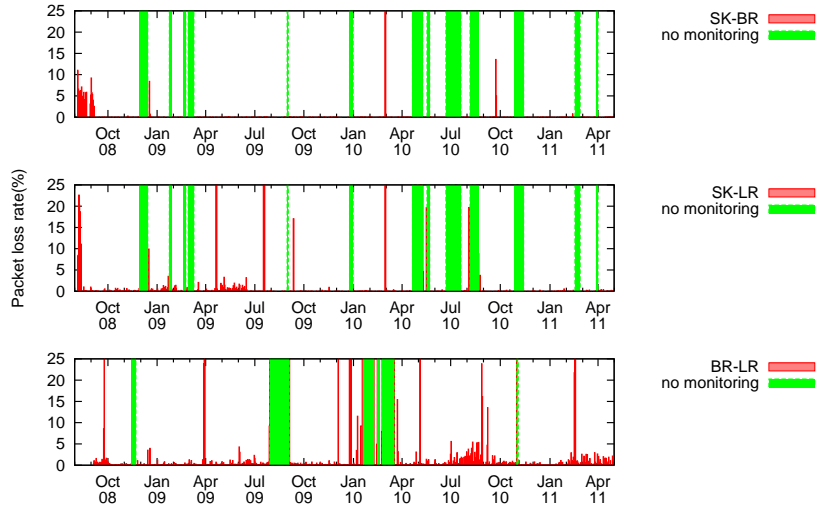


Figure 7: Long-term stability of the network from August 2008. Red histograms in the top two panels show daily packet loss rate in the line between the SK to BR towers and in the line between the SK to LR towers, respectively. The bottom panel shows the same in the line between the BR and LR FD stations. The monitor data for daily packet loss rate were not recorded in the green regions.

256 range. The line between the SK and BR towers and the line between the SK
 257 and LR towers are used for SD data acquisition. No access to FD stations
 258 and CLF for general purposes interferes with the SD data acquisition lines.
 259 The long distance networks are currently operated at 3 Mbps throughput,
 260 which is sufficient for SD data acquisitions, data transfer and operation of
 261 FD stations.

262 Fig. 7 shows the daily average values of packet loss rate in the lines
 263 monitored in the current system. The network is stable enough, except for
 264 some periods of major maintenances. More details of long distance network

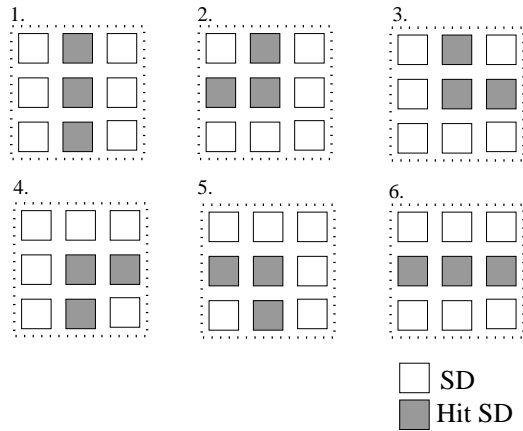


Figure 8: Trigger pattern taken at the TA surface array. If any three adjacent SDs have Level-1 trigger, timing differences are within $8 \mu\text{sec}$ of which the Level-2 trigger will be generated.

265 in the TA experiment are described in papers [18, 19].

266 4. Data communication and air shower trigger

267 There is a trigger-decision module at each tower. The electronics is the
 268 same as shown in Fig. 4, running a different firmware program. The data
 269 communication between the trigger-decision electronics at communication
 270 tower and SDs is done by 2.4 GHz wireless LAN using a custom-made com-
 271 munication protocol. The baud rate of the data acquisition is ~ 1 Mbps.
 272 Every second, the trigger-decision electronics at the communication tower
 273 requests each surface detector to send a Level-1 trigger event list and the
 274 total counts of the sub-clock between PPS signals. From the event lists, an
 275 air shower trigger is generated when three adjacent SDs are coincident within
 276 $8 \mu\text{sec}$. Fig. 8 shows the current trigger pattern of three adjacent SDs that

277 are hit. We call this trigger the Level-2 trigger. With this trigger, collec-
278 tion of waveforms stored in each SD electronics starts. The trigger-decision
279 electronics collects waveforms coincident within $\pm 32 \mu\text{sec}$ from the trigger
280 timing. When the Level-2 trigger is generated within one subarray, the trig-
281 ger time information is transmitted to the central trigger decision process.
282 The process is running at the data acquisition PC (TS7800; Technologic sys-
283 tems, Co. Ltd.) in the SK tower. From the SK tower, the Level-2 trigger
284 signal is distributed to other two towers. The broadcasting of this trigger en-
285 ables to collect waveforms associated with a shower which impacts multiple
286 subarrays. Fig. 9 shows an event triggered at BR subarray. Fig. 10 shows
287 a sample of waveforms.

288 To collect air shower event at the boundary of subarrays, the Level-1 trigger
289 event lists from the SDs at the boundary of subarrays are also sent to the
290 central trigger process in SK tower. The central trigger process combines
291 Level-1 trigger information collected from SDs at the boundary of subarrays.
292 The central trigger process verifies whether the same trigger condition was
293 satisfied only by the boundary detectors.

294 As shown in Fig. 8, in the case of pattern 1 or 6, the hit pattern that sat-
295 isfies the Level-2 trigger condition can be spread over 2 subarrays, but the
296 condition is not satisfied with edge detectors only. To trigger such a case,
297 central trigger process searches for the coincidence of two adjacent hits in
298 the boundary detectors from Level-1 trigger list. If such a coincidence exists,
299 the central trigger process sends time and position information of the coinci-
300 dence to all towers. Trigger-decision electronics at towers verify the Level-2
301 trigger condition using the received information from the central trigger pro-

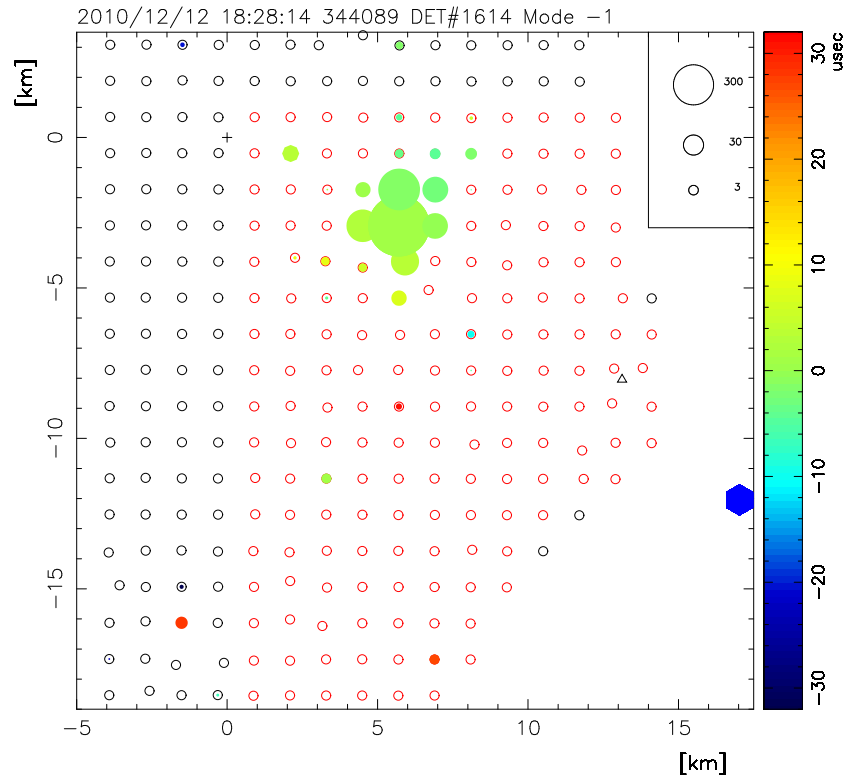


Figure 9: An example of triggered event at BR array. Red open circles represent SDs in BR subarray. The triggered SDs are shown with color code, which corresponds to the arrival time. The radius of a circle is proportional to the logarithm of the integrated signal amount in the unit of MIP.

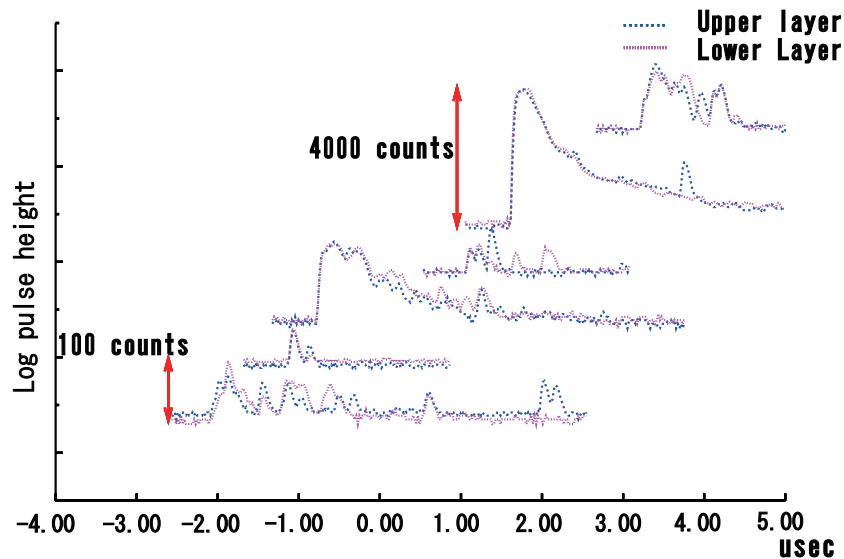


Figure 10: Waveforms obtained from the event shown in Fig. 9

302 cess. Shower events of relatively small size that fall near the boundary of
 303 subarrays is collected by this trigger scheme.

304 With the above trigger conditions, trigger efficiency reaches 97% for pri-
 305 mary particle with energy of $10^{19.0}$ eV. Here the efficiency includes the effect
 306 of dead counters [16, 20, 23]. Fig. 11 shows trigger efficiency as a function of
 307 energy of primary particle obtained using CORSIKA [24] air shower Monte
 308 Carlo simulation and GEANT4 [25] detector Monte Carlo simulation [26].

309 To improve the efficiency of detecting FD-SD hybrid events at lower ener-
 310 gies ($< 10^{18.7}$ eV), an external trigger called Hybrid Trigger was installed to
 311 collect waveforms associated with air showers detected by FD. From nearest
 312 FD, the SD data acquisition system at a tower receives trigger timing and
 313 time window for requesting waveforms stored at each SD in the subarray.
 314 The efficiency of the waveform collection is greater than 97% for the primary

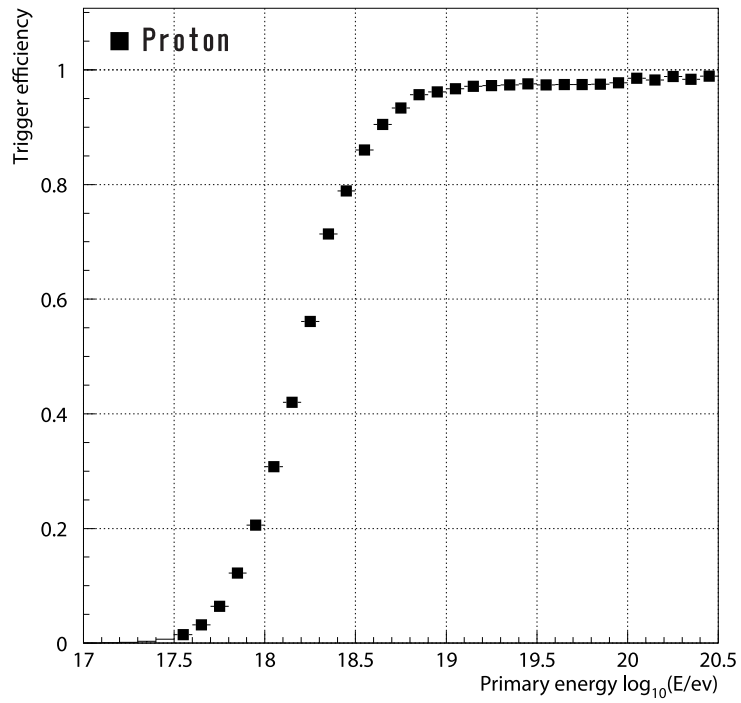


Figure 11: Trigger efficiency as a function of energy for primary proton calculated using CORSIKA air shower Monte Carlo simulation and GEANT4 detector Monte Carlo simulation.

315 particle with energy of $10^{17.5}$ eV triggered by FD [27]. The extended hybrid
 316 trigger observations started in October 2010.

317 5. Detector Calibration and Monitoring

318 For stable observation, the status and environment of the batteries need
 319 to be monitored continuously. For calibration in later analysis, it is very
 320 important to monitor the detector response. For this purpose, a monitoring
 321 process runs on each SD in a 10 min cycle. The monitored items are summa-
 322 rized in Table 1 [28]. The size of monitoring data for 10 min is 9600 bytes.
 323 The data is divided into 600 subsets. All the subsets are sent along with the
 324 Level-1 trigger tables within 10 min.

Table 1: Items and resolutions of TA Surface Detector monitor.

Item	Data	Resolution
1MIP histogram	12bin sum of FADC	1 FADC count 10min
Pedestal histogram	8bin sum of FADC	1 FADC count 10min
Pulse height histogram	Maximum FADC	32 FADC count 10min
Total charge histogram	128bin sum of FADC	$\Delta \log_2(\text{FADC sum})=0.2$
Power cycle data	Battery (voltage, current)	1min
Environmental data	Temperature, humidity	1min
Trigger rate	Level-0, Level-1 trigger rate	1min
GPS status	Number of satellites, status	10min

325 5.1. The 1-MIP monitor

326 The charge output by atmospheric charged particles is used to estimate
 327 the total energy deposited by shower particles. The integrated FADC value

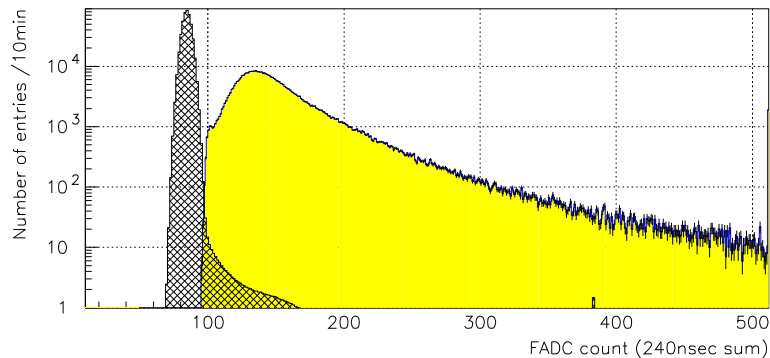


Figure 12: Example of FADC count distribution from Level-0 trigger events obtained as 1-MIP monitor data. The hatched histogram is a pedestal distribution collected as monitor data. The pedestal distribution is scaled to have the same entry as the Level-0 trigger data. The same distribution is collected from every PMT at 10 min intervals.

328 recorded by the Level-0 trigger is collected as monitoring data from each
 329 surface detector. Here the time window for the integration is 240 nsec (12
 330 bins). The time window ranges between -4 bins from trigger timing and +8
 331 bins after trigger timing. That is sufficient to evaluate MIP peak count of
 332 FADC. Fig. 12 shows an example of the charge output distribution. The
 333 last bin of the histogram is the overflow bin. The temperature coefficient
 334 of gain of the surface detectors is typically $-0.8\%/^{\circ}\text{C}$ for a diurnal variation
 335 of temperature that reaches up to 25°C [21]. Fig. 13 shows examples of
 336 the monitored time variations of temperature, relative humidity inside the
 337 scintillator box, and 1-MIP peak value. Change of detector response caused
 338 mainly by the variation of the outside temperature is monitored by this
 339 distribution continuously to the nearest ten minutes.

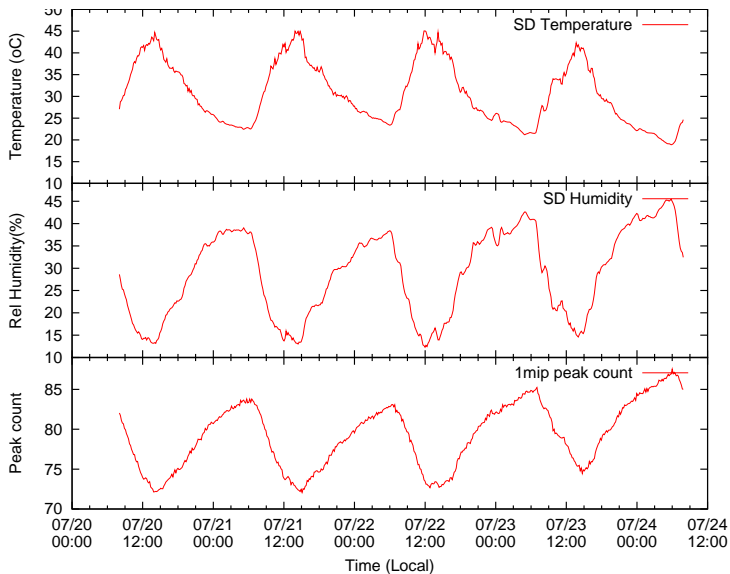


Figure 13: Examples of time variations of temperature (top) and relative humidity (middle) inside the scintillator box, and the 1-MIP peak value (bottom).

340 *5.2. Linearity monitor*

341 A check on the linearity of charge output was performed by using two
 342 LEDs attached at each layer of scintillator. This was done for all the detectors
 343 before deployment. Two LEDs were flashed with 400 nsec wide square pulses
 344 alternately or simultaneously. The amount of light from each LED is changed
 345 by changing the pulse height of the square pulse. From the ratio of the
 346 measured output to the expected output, the linearity curves were measured.
 347 Here we describe the light amount as x and the peak of the pulse from a
 348 PMT in FADC count as $F(x)$ while driving one LED. The PMT output
 349 while driving LED 1 and 2 simultaneously is represented as $F(x_1 + x_2)$. The
 350 linearity was checked by comparing $F(x_1 + x_2)$ and $F(x_1) + F(x_2)$ while
 351 changing x_1 and x_2 . Fig. 14 shows a typical example of observed relation

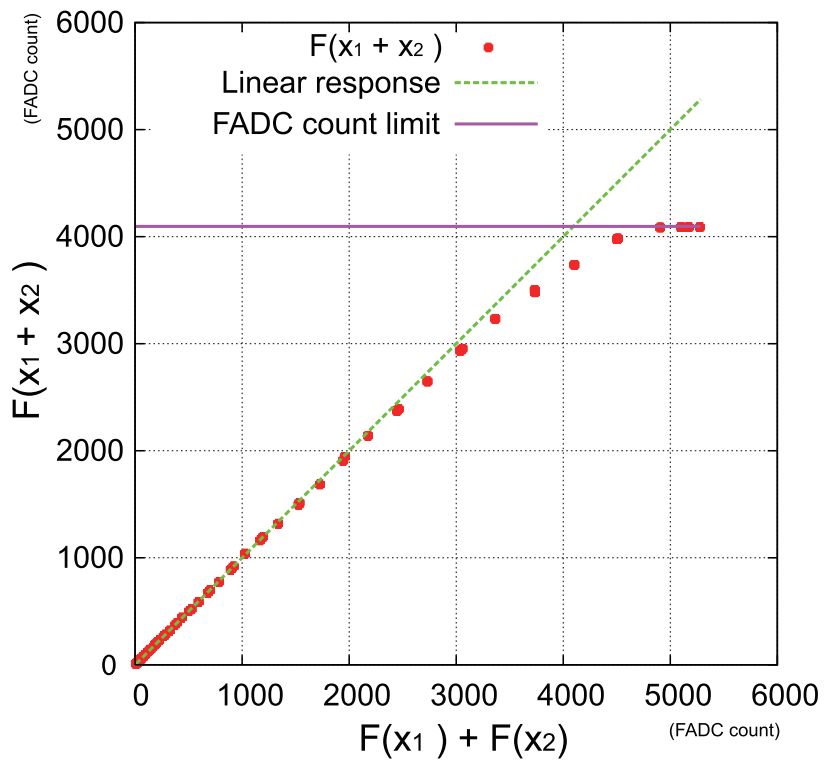


Figure 14: An example of observed relation between $F(x_1 + x_2)$ and $F(x_1) + F(x_2)$.

352 between $F(x_1 + x_2)$ and $F(x_1) + F(x_2)$.

353 To check the linearity and its variation in the long term of operation,
354 pulse-height (FADC peak) histograms are also taken as monitoring data.
355 The pulse height of the signal that satisfies the level-0 trigger condition is
356 counted into a histogram. The high voltage values of the PMTs of all the
357 detectors are adjusted to obtain almost the same FADC counts for 1 MIP
358 peaks. So the histograms differ between detectors because of the difference of
359 the linearity of the PMTs. We monitor the histogram to detect time variation
360 of the linearity. By comparing the tail of the histogram and the one from
361 the tubes with good linearity, it is possible to estimate non-linearity. Fig. 15
362 shows an example of comparison between pulse-height linearity obtained from
363 LED calibration and the one estimated using the pulse-height monitor. It
364 shows fairly good agreement and it was confirmed that the histogram can be
365 used for monitoring the stability of linearity. When the pulse height of signal
366 is larger than the expected height of saturation, the signal is not used for
367 analyzing lateral distribution of shower particle. But the timing information
368 is used for calculating arrival direction.

369 *5.3. Power monitor, GPS and environmental parameters*

370 Since each SD is locally powered by a solar panel and a battery, it is very
371 important to monitor the status of the output voltage and current from the
372 battery. The 1PPS signals are generated by GPS modules using the signals
373 from the satellites that are visible through the GPS antennas. To understand
374 the status of the GPS module, the number of satellites visible through the
375 GPS module and conductivity of the antenna are read out every 600 sec.
376 Each surface detector is equipped with five temperature sensors and two

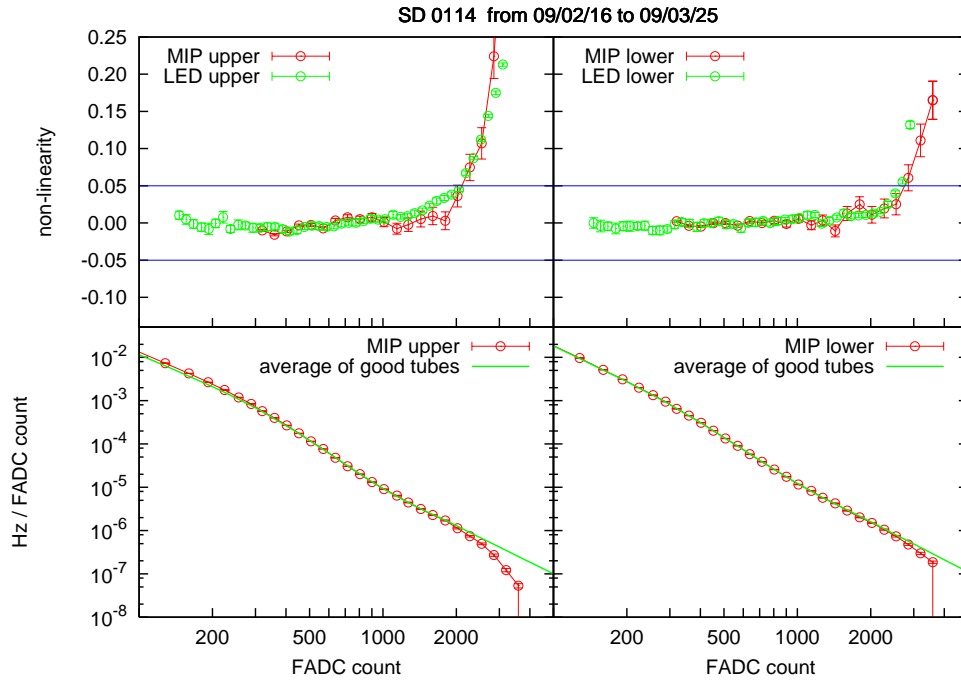


Figure 15: Analyzed linearity of pulse height from monitor data [16]. In the top left panel, the green open circles denote the relative deviation from the estimated linear response by LED calibration, and the red open circles denote the relative deviation by pulse-height monitor for the upper layer of one SD (SD #0114). The top right panel shows the same for the lower layer. In the bottom left panel, the red open circles denote the scaled pulse height distribution observed for the upper layer, and the green line denotes the average from good tubes. The bottom right panel shows the same for the lower layer.

377 humidity sensors to record the environment of the detector and electronics
378 box.

379 Fig. 16 gives an example of the time variations in the number of de-
380 tected GPS satellites, the battery voltage and charging current, the Level-0
381 and Level-1 trigger rates for one detector, and the barometric pressure and
382 atmospheric temperature measured at the CLF [17] site.

383 **6. Summary**

384 The SD array of the TA experiment consists of 507 plastic scintillation
385 detectors of 3 m² in size. The array has the largest total area in the northern
386 hemisphere. The detector enables us to compare estimated energy of primary
387 particle using longitudinal shower development observed at FD and lateral
388 distribution of shower particles detected with the SD array. The observation
389 with the SD array is continuous to have ~100% of duty cycle. This feature
390 enables us to explore the anisotropy of arrival directions of highest energy
391 cosmic rays with larger exposure than observation with FD.

392 The deployment of the surface detectors started in October 2006. Totally
393 507 surface detectors were deployed by November 2008. The deployed detec-
394 tors have been calibrated and tuned. The air shower array began operation
395 in March 2008. For more than three years, air shower events from UHECR
396 have been collected along with detailed monitoring data. The monitoring
397 data enables us to calibrate the variation of detector responses with enough
398 accuracy. We showed the running status after three years of SD operation.
399 An upgrade of the DAQ system was performed and additional deployment
400 was made in November 2008. Including maintenance periods, the array has

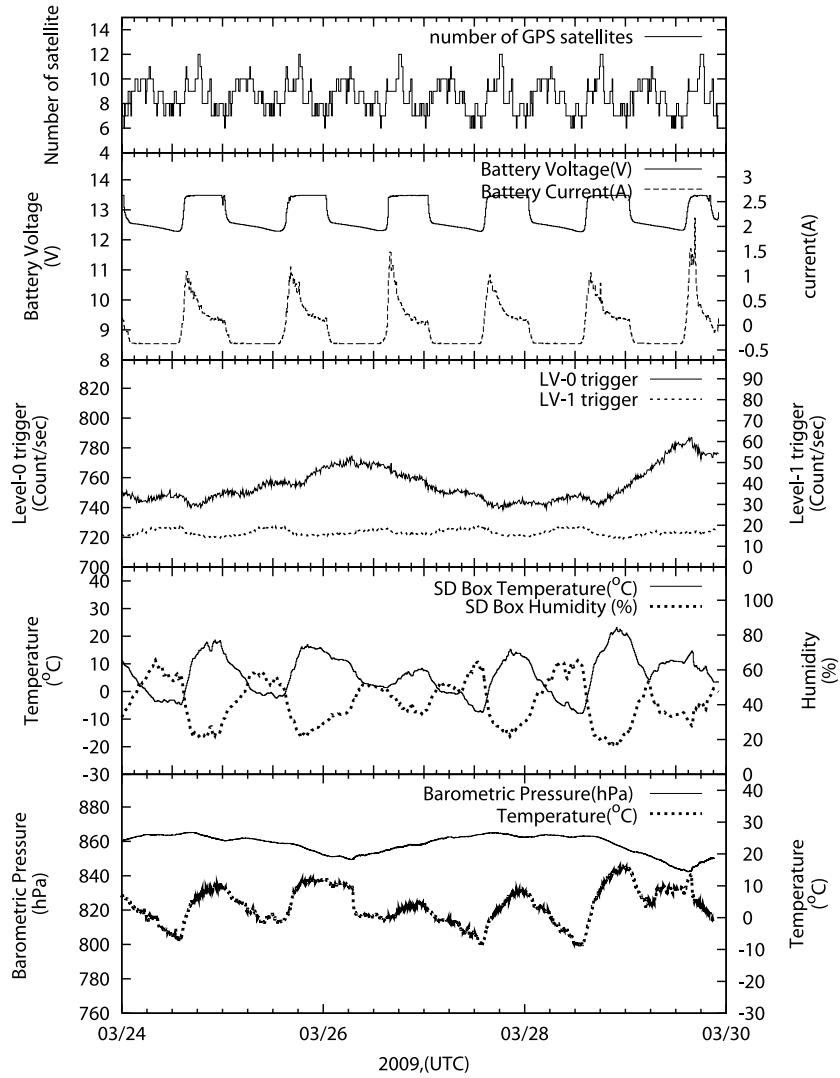


Figure 16: An example of time variations in the number of GPS satellites (top panel), battery voltage and charging current (second panel), local Level-0 and Level-1 trigger rates (third panel) for one surface detector, and the barometric pressure and atmospheric temperature measured at the CLF site using a weather transmitter (WXT510; VAISALA Inc.)(bottom panel).

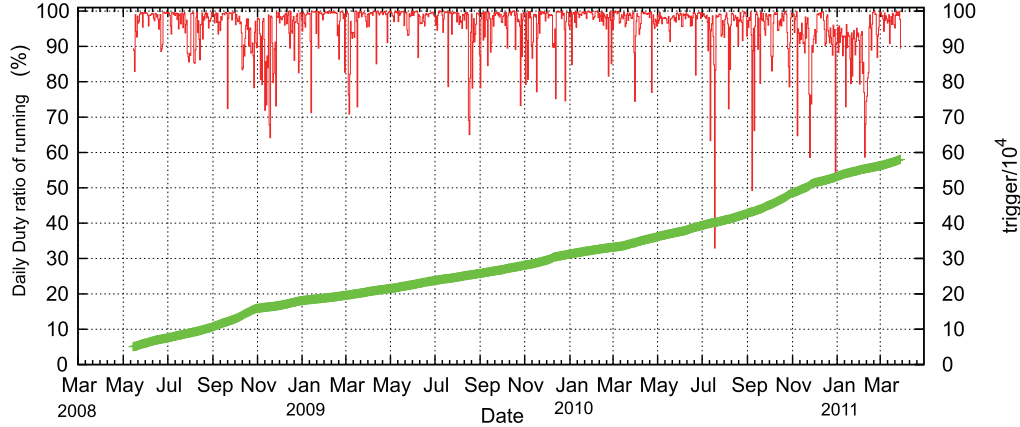


Figure 17: Running status of the SD array. Daily duty ratio of running. Evolution of the number of triggered event is also shown using right vertical axis.

401 been operating with a 95% of duty cycle on average. The variations of de-
 402 tector response and status are recorded in 10 min resolution and are well
 403 understood. The number of triggers collected as of March 2011 has reached
 404 5×10^5 .

405 Acknowledgments

406 The Telescope Array experiment is supported by the Japan Society for
 407 the Promotion of Science through Grants-in-Aid for Scientific Research on
 408 Specially Promoted Research (21000002) “Extreme Phenomena in the Uni-
 409 verse Explored by Highest Energy Cosmic Rays”, and the Inter-University
 410 Research Program of the Institute for Cosmic Ray Research; by the U.S.
 411 National Science Foundation awards PHY-0307098, PHY-0601915, PHY-
 412 0703893, PHY-0758342, and PHY-0848320 (Utah) and PHY-0649681 (Rut-

413 gers); by the National Research Foundation of Korea (2006-0050031, 2007-
414 0056005, 2007-0093860, 2010-0011378, 2010-0028071, R32-10130, 2011-0002617);
415 by the Russian Academy of Sciences, RFBR grants 10-02-01406a and 11-
416 02-01528a (INR), IISN project No. 4.4509.10 and Belgian Science Policy
417 under IUAP VI/11 (ULB). The foundations of Dr. Ezekiel R. and Edna
418 Wattis Dumke, Willard L. Eccles and the George S. and Dolores Dore Ec-
419 cles all helped with generous donations. The State of Utah supported the
420 project through its Economic Development Board, and the University of
421 Utah through the Office of the Vice President for Research. The experi-
422 mental site became available through the cooperation of the Utah School
423 and Institutional Trust Lands Administration (SITLA), U.S. Bureau of Land
424 Management and the U.S. Air Force. We also wish to thank the people and
425 the officials of Millard County, Utah, for their steadfast and warm support.
426 We gratefully acknowledge the contributions from the technical staffs of our
427 home institutions and the University of Utah Center for High Performance
428 Computing (CHPC).

429 **References**

- 430 [1] H. Kawai, et al., Nucl. Phys. Proc, suppl, vol 175-176 (2008) 221-226.
- 431 [2] M. Takeda, et al., Phys. Rev. Lett. 81 (1998) 1163.
- 432 [3] M. Takeda, et al., Astroparticle Physics 19 4 (2003) 447.
- 433 [4] K. Greisen, Phys. Rev. Lett. 16 (1966) 748.
- 434 [5] T. Zatsepin and V.A.Kuzmin, JETP Lett 4 (1966) 178.

- 435 [6] T. Abu-Zayyad, et al., Phys. Rev. Lett. 92 (2004) 151101.
- 436 [7] J. Abraham, et al., Phys. Rev. Lett. 101 (2008) 061101.
- 437 [8] N. Hayashida, et al., Astroparticle Physics 10 (1999) 303-311.
- 438 [9] J.N. Matthews, et al., Proceedings of the 30th International Cosmic Ray
439 Conference in Merida Vol.4 (2007) 417-420 .
- 440 [10] T. Shibata, et al., Proceedings of the 30th International Cosmic Ray
441 Conference in Merida Vol.5 (2007) 1069-1072 .
- 442 [11] T. Shibata, et al., Nucl. Instrum. Methods Phys. Res., Sect, A 597, 61
443 (2008).
- 444 [12] I. Tkachev, et al., Proceedings of the 31th International Cosmic Ray
445 Conference in Beijing ID 1311 (2011).
- 446 [13] T. Tomida, Master thesis University of Yamanashi (2008).
- 447 [14] S. Kawakami, et al., Proceedings of the 29th International Cosmic Ray
448 Conference in Pune 8 (2005) 161.
- 449 [15] S. Yoshida, et al., Proceedings of the 29th International Cosmic Ray
450 Conference in Pune 8 (2005) 2411.
- 451 [16] A. Taketa, et al., Proceedings of the 31th International Cosmic Ray
452 Conference in Łódź ID 924 (2009).
- 453 [17] S. Udo, et al., Proceedings of the 30th International Cosmic Ray Con-
454 ference in Merida Vol.5 (2007) 1021.

- 455 [18] T. Nonaka et al., Proceedings of the 31th International Cosmic Ray
456 Conference C in Łódź ID 977 (2009).
- 457 [19] S. Iwamoto, Master thesis University of Yamanashi (2009).
- 458 [20] N.Sakurai, et al., Proceedings of the 30th International Cosmic Ray
459 Conference in Merida, Vol.5 (2007) 1159.
- 460 [21] T. Nonaka, et al., Proceedings of the 30th International Cosmic Ray
461 Conference in Merida, Vol 5 (2007) 1005.
- 462 [22] A. Taketa, et al., in preperation.
- 463 [23] Y. Yamakawa, Master thesis University of Tokyo (2009).
- 464 [24] D. Heck, et al., Forschungszentrum Karlsruhe Report FZKA 6019
465 (1998).
- 466 [25] S. Agostinelli, et al., Nuclear Instruments and Methods in Physics Re-
467 search A 506 (2003) 250-303.
- 468 [26] B. Stokes, et al., Proceedings of the 31th International Cosmic Ray
469 Conference in Łódź ID 1328 (2009).
- 470 [27] R. Ishimori, et al., Proceedings of International Symposium on the Re-
471 cent Progress of Ultra-high Energy Cosmic Ray Observation, Nagoya
472 (2010).
- 473 [28] T. Nonaka, et al., Proceedings of the 31th International Cosmic Ray
474 Conference C in Łódź ID 974 (2009).